UNIVERSITY OF AMSTERDAM

UvA-DARE (Digital Academic Repository)

Non-Invasive, Bioluminescence-Based Visualisation and Quantification of Bacterial Infections in Arabidopsis Over Time

Taks, N.W.; Batstra, M.D.; Kortekaas, R.F.; Stevens, F.D.; Pfeilmeier, S.; van den Burg, H.A.

DOI
10.1111/mpp.70055

Publication date
2025

Document Version
Final published version

Published in
Molecular Plant Pathology

License
CC BY-NC

Link to publication

Citation for published version (APA):
Taks, N. W., Batstra, M. D., Kortekaas, R. F., Stevens, F. D., Pfeilmeier, S., & van den Burg, H. A. (2025). Non-Invasive, Bioluminescence-Based Visualisation and Quantification of Bacterial Infections in *Arabidopsis* Over Time. *Molecular Plant Pathology*, *26*(2), Article e70055. https://doi.org/10.1111/mpp.70055

General rights
It is not permitted to download or to forward/distribute the text or part of it without the consent of the author(s) and/or copyright holder(s), other than for strictly personal, individual use, unless the work is under an open content license (like Creative Commons).

Disclaimer/Complaints regulations
If you believe that digital publication of certain material infringes any of your rights or (privacy) interests, please let the Library know, stating your reasons. In case of a legitimate complaint, the Library will make the material inaccessible and/or remove it from the website. Please Ask the Library: https://uba.uva.nl/en/contact, or a letter to: Library of the University of Amsterdam, Secretariat, P.O. Box 19185, 1000 GD Amsterdam, The Netherlands. You will be contacted as soon as possible.

UvA-DARE is a service provided by the library of the University of Amsterdam (https://dare.uva.nl)

Download date:13 Nov 2026

Check for updates

Molecular Plant Pathology

WILEY

Molecular Plant Pathology

TECHNICAL ADVANCE OPEN ACCESS

Non-Invasive, Bioluminescence-Based Visualisation and Quantification of Bacterial Infections in *Arabidopsis* Over Time

Nanne W. Taks[1] | Mathijs D. Batstra[2] | Ronald F. Kortekaas[2] | Floris D. Stevens[1] | Sebastian Pfeilmeier[1] | Harrold A. van den Burg[1,3]

[1]Molecular Plant Pathology, Swammerdam Institute for Life Sciences, Faculty of Science, University of Amsterdam, Amsterdam, Netherlands | [2]Technology Center FNWI, Faculty of Science, University of Amsterdam, Amsterdam, Netherlands | [3]Rijk Zwaan Zaadteelt en Zaadhandel B.V, Burgemeester Crezéelaan 40, De Lier, Netherlands

Correspondence: Harrold A. van den Burg (h.a.vandenburg@uva.nl)

Received: 9 October 2024 | **Revised:** 14 December 2024 | **Accepted:** 3 January 2025

Funding: This work was supported by NWO (OCENW.XS24.1.155), Topsector T&U (EZ-2012-02, TU18024), Rijk Zwaan and Bejo Zaden B.V.

Keywords: *Arabidopsis thaliana* | automated image analysis | bioluminescence | non-invasive phenotyping | phytopathogenic bacteria | plant resistance | *Xanthomonas campestris*

ABSTRACT

Plant-pathogenic bacteria colonise their hosts using various strategies, exploiting both natural openings and wounds in leaves and roots. The vascular pathogen *Xanthomonas campestris* pv. *campestris* (Xcc) enters its host through hydathodes, organs at the leaf margin involved in guttation. Subsequently, Xcc breaches the hydathode–xylem barrier and progresses into the xylem vessels causing systemic disease. To elucidate the mechanisms that underpin the different stages of an Xcc infection, a need exists to image bacterial progression in planta in a non-invasive manner. Here, we describe a phenotyping setup and Python image analysis pipeline for capturing 16 independent Xcc infections in *Arabidopsis thaliana* plants in parallel over time. The setup combines an RGB camera for imaging disease symptoms and an ultrasensitive CCD camera for monitoring bacterial progression inside leaves using bioluminescence. The method reliably quantified bacterial growth in planta for two bacterial species, that is, vascular Xcc and the mesophyll pathogen *Pseudomonas syringae* pv. *tomato* (Pst). The camera resolution allowed Xcc imaging already in the hydathodes, yielding reproducible data for the first stages prior to the systemic infection. Data obtained through the image analysis pipeline was robust and validated findings from other bioluminescence imaging methods, while requiring fewer samples. Moreover, bioluminescence was reliably detected within 5 min, offering a significant time advantage over our previously reported method with light-sensitive films. Thus, this method is suitable to quantify the resistance level of a large number of *Arabidopsis thaliana* accessions and mutant lines to different bacterial strains in a non-invasive manner for phenotypic screenings.

1 | Introduction

Plants are colonised by a wide range of pathogenic microbes that apply different strategies to infect plant tissues (Jian et al. 2024). To study these interactions, it is important to reliably quantify plant susceptibility to a specific pathogen. For phytopathogenic bacteria, such as the model pathogen *Pseudomonas syringae* pv. *tomato* (Pst), standard phenotyping methods still rely on visual assessment of plant responses and the quantification of bacterial colonisation via colony-forming units (CFUs) (Tornero and Dangl 2001; Whalen et al. 1991). While these methods typically provide highly accurate evaluations of the level of plant disease resistance and susceptibility, they are often labour-intensive and destructive. This poses challenges when studying pathogens that

This is an open access article under the terms of the Creative Commons Attribution-NonCommercial License, which permits use, distribution and reproduction in any medium, provided the original work is properly cited and is not used for commercial purposes.

© 2025 The Author(s). *Molecular Plant Pathology* published by British Society for Plant Pathology and John Wiley & Sons Ltd.

follow a multistaged infection process across different tissues, as these methods often disregard spatial interactions over time. A prime example can be found in the vascular bacterial pathogen *Xanthomonas campestris* pv. *campestris* (Xcc), an economically relevant pathogen of cabbage that shows several distinct stages during its infection cycle (Cerutti et al. 2017; Paauw et al. 2023). As its initial entry point into plant tissue, this specialised bacterium exploits hydathodes, which are gland-like structures at the leaf margin that excrete xylem sap in a process called guttation (Cerutti et al. 2017; Hugouvieux, Barber, and Daniels 1998). Inside the hydathode, the bacteria are found to proliferate for up to a week (depending on the level of plant resistance) without causing any visual disease symptoms (Paauw et al. 2023). They then transit into the xylem vessels that protrude into the hydathode tissue and systemically spread from these points to the rest of the leaf vasculature (Cerutti et al. 2017; Paauw et al. 2023). Earlier work has shown that *Arabidopsis thaliana* (hereafter Arabidopsis) displays an immune response in both the hydathodes and vasculature upon Xcc recognition, which restricts bacterial spread at different stages of the infection (Lin et al. 2022; Paauw et al. 2023; Taks et al. 2024; Wang et al. 2015). To study the mechanism underpinning Xcc colonisation of different tissues in Arabidopsis, a need exists to develop imaging methods that allow us to capture the entire infection process in one individual plant over time in a non-invasive manner.

Currently, methods to quantify the spread and proliferation of Xcc in Arabidopsis include manual scoring of disease symptoms using indices (Guy et al. 2013; Meyer et al. 2005; Wang et al. 2015), inferring the bacterial titre from sections of leaf tissue (Feng et al. 2012; Guy et al. 2013; Lin et al. 2022; Wang et al. 2015) and measuring the length of the V-shaped chlorotic lesions (Xie et al. 2023), a typical disease symptom caused by Xcc. Although these methods provide sufficient accuracy, they disregard hydathode colonisation as a critical initial stage of the infection. In recent years, efforts have been made to visualise Xcc in hydathodes by using foremost bacterial reporter systems such as bioluminescence. Application of an engineered *luxCDABE* operon from *Photorhabdus luminescens* (Winson et al. 1998) has proven successful in visualising Xcc in Arabidopsis hydathodes (Cerutti et al. 2017; Paauw et al. 2024, 2023; van Hulten, Chatterjee, and van den Burg 2019). However, the quantification of hydathode colonisation is still labour-intensive as the sampling methods remained destructive (single leaf detachment). Hence, valuable data on the ability of the bacteria to spread from hydathode to the vascular system cannot be captured using repeated measures on the same plant. Therefore, non-invasive methods for visualising early hydathode infections and subsequent colonisation of leaf tissue are needed.

Non-invasive imaging of luminescence is typically done using a highly sensitive charge-coupled device (CCD) camera. While often used for detection of horseradish peroxidase (HRP) activity in immunoblots, it has also been successfully applied to detect a range of pathogenic bacteria in plants (Furci, Pascual-Pardo, and Ton 2021; Jutras et al. 2021; Mutka et al. 2016; Soldan et al. 2021; Wang et al. 2024; Xu et al. 2022). Although many laboratories are equipped with CCD camera setups, they are not suited to process large plant populations due to size constraints of the device. However, to be able to fully exploit the genetic diversity and resources that are available for Arabidopsis (Simon et al. 2008; Van de Weyer et al. 2019; Weigel and Mott 2009), high-throughput devices are needed to effectively screen large groups of plants. For instance, the resistance gene *SUPPRESSOR OF TOPP4 1* (*SUT1*) that acts in hydathodes against infection by Xcc (Taks et al. 2024) was identified by screening thousands of individual plants and evaluating the level of resistance by manual scoring of a luminescence index (van Hulten, Chatterjee, and van den Burg 2019). To surpass such labour-intensive and bias-prone methods, a bioluminescence imaging setup that enables screening of a plant population would significantly speed up these processes.

Quantification of bioluminescence is often performed using manual annotation of the images—either in proprietary software (Furci, Pascual-Pardo, and Ton 2021; Xu et al. 2022) or ImageJ (Jutras et al. 2021; Mutka et al. 2016; Soldan et al. 2021; Wang et al. 2024)—or with a routine image analysis pipeline. To avoid manual errors/bias, automated image analysis pipelines have been developed in ImageJ (Laflamme et al. 2016) and the OpenCV image analysis library in Python (Paauw et al. 2024). These pipelines offer fast quantification of disease symptoms or bacterial luminescence but require highly standardised input images. To acquire such images, plants need to be imaged in a rigid setup to allow for smooth image analysis processing. Therefore, a tailored system is required to be able to combine the power of bioluminescence and automated image analysis processing.

Here, to develop a system that enables both the tracking of the entire Xcc infection process in Arabidopsis and screening of large plant populations, a custom-made imaging cabinet was designed. This cabinet contains a dual camera, RGB and CCD, and allows for the successive imaging of the plants and the bioluminescence emitted by the bacteria inside these plants. In addition, we designed imaging trays that can hold 16 Arabidopsis rosettes in a grid allowing fully automated image processing. Finally, we developed a Python analysis pipeline to quantify both disease symptoms and bacterial spread. Here, we benchmark this method for Xcc and show that it can also be applied for other phytopathogenic bacteria. Our method holds promise for uncovering intricate mechanisms that happen in a highly localised and temporal basis during plant–pathogen interactions.

2 | Results

2.1 | How to Build a Digital Phenotyper: Designing the Hardware

To assess disease severity caused by an Xcc infection, the procedure thus far involved spray inoculation of Arabidopsis plants and artificial humidity/temperature cycles to promote guttation and uptake of Xcc in hydathodes (van Hulten, Chatterjee, and van den Burg 2019). Using a bioluminescent Xcc reporter strain, we then monitored bacterial spread in planta for up to 14 days post-inoculation (dpi) (Figure 1A). To unravel the complex interactions involving different host tissue types, that is, hydathodes, xylem vessels and mesophyll, we developed a non-invasive method for imaging bacterial infection in a spatiotemporal manner. To this end, a custom-made phenotyping cabinet was designed that features white LEDs and two digital cameras, that is,

13643703, 2025, 2, Downloaded from https://bsppjournals.onlinelibrary.wiley.com/doi/10.1111/mpp.70055 by Uva Universiteitsbibliotheek, Wiley Online Library on [10/02/2025]. See the Terms and Conditions (https://onlinelibrary.wiley.com/terms-and-conditions) on Wiley Online Library for rules of use; OA articles are governed by the applicable Creative Commons License

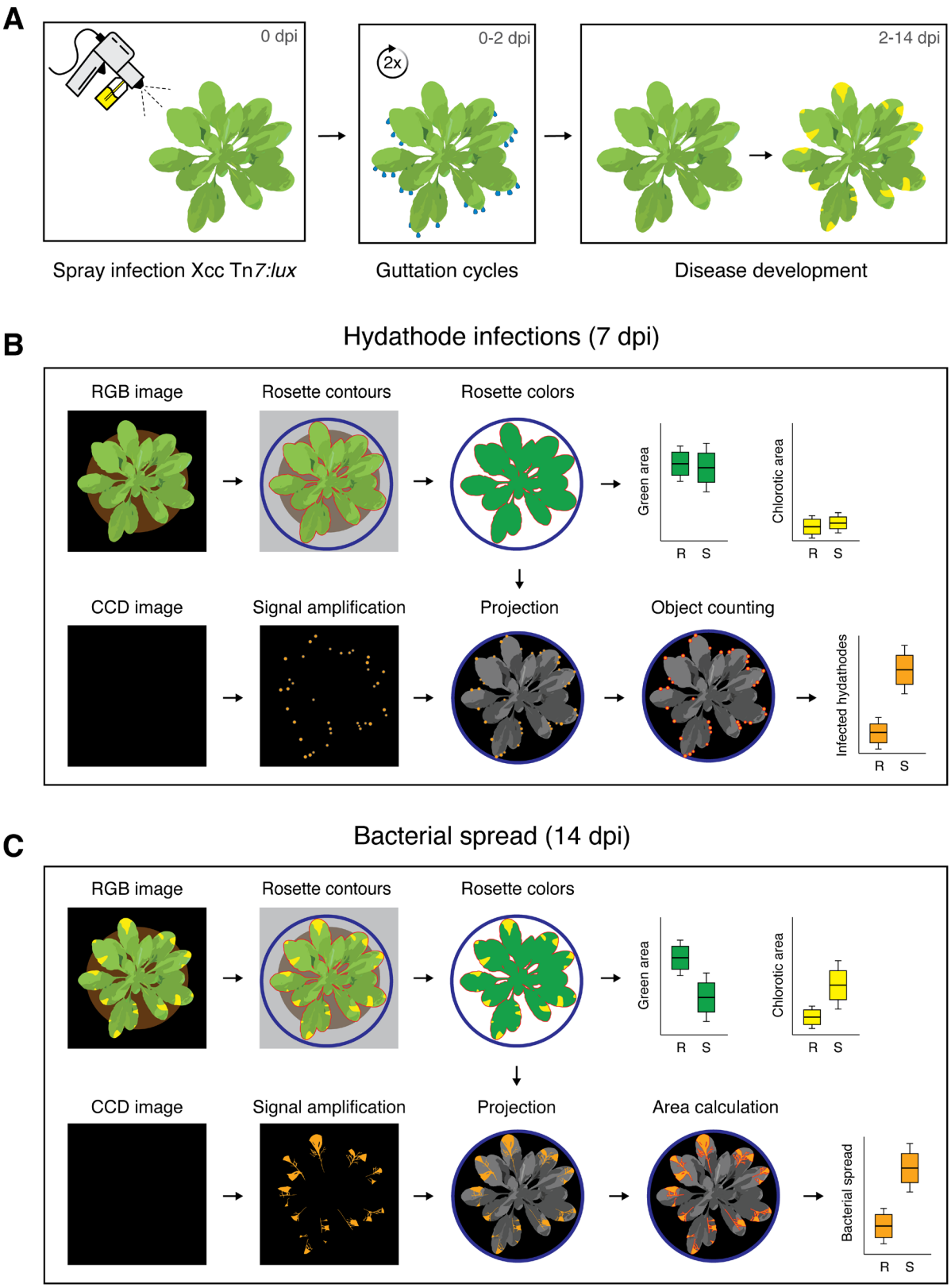

FIGURE 1 | Schematic representation of the spray inoculation procedure with *Xanthomonas campestris* pv. *campestris* (Xcc) Tn*7*:*lux* and the subsequent image analysis pipeline. (A) Spray inoculation procedure with Xcc Tn*7*:*lux* mimics natural infection via hydathodes. (B) Schematic overview of the pipeline for quantification of infected hydathodes per rosette at 7 days post-inoculation (dpi) resulting in number of infected hydathodes, total rosette area and chlorotic area as outputs. R, resistant; S, susceptible. (C) Schematic overview of pipeline for quantification of disease symptoms and bacterial spread per rosette at 14 dpi resulting in bacterial spread (defined as total luminescent area), total rosette area and chlorotic area as outputs.

13643703, 2025, 2, Downloaded from https://bsppjournals.onlinelibrary.wiley.com/doi/10.1111/mpp.70055 by Uva Universiteitsbibliotheek, Wiley Online Library on [10/02/2025]. See the Terms and Conditions (https://onlinelibrary.wiley.com/terms-and-conditions) on Wiley Online Library for rules of use; OA articles are governed by the applicable Creative Commons License

an RGB camera for rosette imaging and an ultrasensitive CCD camera for bioluminescence imaging (Figure S1A). To avoid internal light reflections, the cabinet interior was painted black. As overlap between the plant rosettes can interfere with the automated image processing and analysis (Laflamme et al. 2016; Paauw et al. 2024), we designed a custom-made 4×4 tray using black anodized aluminium, which allows for the imaging of 16 plants in parallel (Figure S1B). In the case of Xcc infections, this ensures that the rosettes do not overlap until at least 14 dpi. For other applications, in which smaller rosettes are imaged, trays with 40 or more rosettes can fit into the imaging cabinet. Plants can be directly grown in these trays or transferred prior to imaging. In the phenotyping cabinet, plants are imaged by an RGB camera (artificial lighting, 70 ms exposure) and a CCD camera (darkness, 300 s exposure), resulting in two image files capturing the rosette phenotype and the spread of bacterial luminescence, respectively (Figure S1C). These images are then fed into our Python image analysis pipeline to obtain data on the individual plant sizes, disease symptoms (chlorosis) per plant and bacterial spread per plant.

2.2 | Automated Image Analysis Pipeline: Developing the Software

To automatically acquire quantitative data, an image analysis pipeline (Figure 1B,C) was written in Python using the OpenCV Library (Bradski and Kaehler 2000). To start the analysis, the output images from the two cameras were calibrated using a 4×11 asymmetric dots calibration sheet allowing us to overlay both images. In the RGB image, individual rosettes were then detected, outlined and sorted based on user-adjustable HSV colour values and contouring parameters. In addition, the total rosette size and the number of green and yellow pixels were quantified. Next, using the defined rosette contours, the smallest enclosing circle was used as a mask around each rosette for the CCD image. Within each circle, luminescence was quantified by the number of luminescent objects and the luminescent area in pixels. To eliminate noise and artefacts in the CCD image, a luminescent signal was only considered when the pixels fall within a user-defined size range (e.g., minimum two pixels). Finally, all quantified variables for each rosette were saved in a .csv file and an overlayed image (.png file) of the RGB and CCD image was created for visual inspection. The pipeline features an environment file in which the different parameters can be adjusted to optimise the pipeline for other setups. All available parameters, code and instructions for this pipeline are provided on GitHub (https://github.com/MolPlantPathology/Digital_phenotyper).

2.3 | Digital Phenotyping Quantifies Disease Severity at Different Stages of Infection

To confirm the validity of our method, we benchmarked our digital phenotyping pipeline against other well-established methods. To do so, we performed spray inoculations of Xcc8004 Δ*xopAC* Tn*7*:*lux* on three Arabidopsis genotypes that we showed previously to have different levels of disease susceptibility; two natural accessions Col-0 (resistant) and Oy-0 (hypersusceptible) and Col-0 mutant line *sut1-9*, which carries a knockout mutation in the CNL-type plant immune receptor SUT1 and shows an intermediate disease resistance phenotype against Xcc8004 Δ*xopAC* (Paauw et al. 2023; Taks et al. 2024). As the three different levels of resistance against Xcc can already be observed for these genotypes at the first stage of the infection in the hydathodes, it allows us to benchmark the sensitivity of our digital phenotyping setup to detect and quantify immune responses in hydathodes. Using our established detached leaf assay (van Hulten, Chatterjee, and van den Burg 2019), we were able to detect an increased number of hydathode infections for both *sut1-9* and the susceptible accession Oy-0 compared to the resistant control Col-0 at 7 dpi based on the count number of luminescent hydathodes observed per leaf (Figure 2A). In parallel, the number of hydathode infections was quantified per rosette using the new pipeline (Figure 2B). Both methods yielded significant and comparable differences in hydathode colonisation by Xcc between the three Arabidopsis lines. Next, to quantify the level of resistance at later stages of infection (i.e., in the vasculature and mesophyll), the proportion of the leaf area colonised by Xcc was quantified in the detached leaf assay using the ScAnalyzer script (Figure 2C) (Paauw et al. 2024) and with our digital phenotyping setup imaging the whole rosette at 14 dpi (Figure 2D). Again, at 14 dpi, we noted a consistent correlation between the results obtained with the detached leaf assay and the non-invasive imaging of whole rosettes. A significant difference between the genotypes was observed with a smaller sample size (Figure 2B,D; $n = 16$; Table S1) compared to the detached leaf assay (Figure 2A,C; $n = 63$; Table S1) at both timepoints (7 and 14 dpi), indicating a high robustness of our approach. Besides bacterial colonisation, we analysed disease symptoms and compared whether both parameters gave consistent results. Both quantification of chlorotic disease symptoms and bacterial colonisation yielded significant differences between Col-0 and Oy-0 at 14 dpi, with bacterial colonisation resulting in more robust data (Figure S2A), as bacterial spread precedes symptom development (Paauw et al. 2024) (Figure S2B). Therefore, using bacterial colonisation as phenotype can reduce the time between infection and phenotyping to obtain high-resolution data.

While quantification at two defined timepoints yields robust data to assess the level of disease resistance, time-series measurements can capture the bacterial progression in the plant tissues with even more precision (Video S1). Moreover, in the case of Xcc infection in Arabidopsis, by imaging the infections over time, it is possible to study the dynamics of the infection process of individual hydathodes, yielding true single hydathode data (Figure 3). Together, we conclude that this digital phenotyping setup provides consistent data similar to the detached leaf assay using light-sensitive films (Paauw et al. 2024) at different timepoints.

2.4 | Digital Phenotyping Approach Is Flexible and Applicable to Mesophyll Pathogens

Although our pipeline was optimised for the interaction between Xcc and Arabidopsis, we assessed its versatility using the model organism Pst strain DC3000 (PstDC3000) to look at stomatal infections in Arabidopsis (Melotto et al. 2017). Arabidopsis Col-0 is susceptible to PstDC3000 (Velásquez et al. 2017). To infer the ability of our pipeline to quantify resistance to Pst, a

13643703, 2025, 2, Downloaded from https://bsppjournals.onlinelibrary.wiley.com/doi/10.1111/mpp.70055 by Uva Universiteitsbibliotheek, Wiley Online Library on [10/02/2025]. See the Terms and Conditions (https://onlinelibrary.wiley.com/terms-and-conditions) on Wiley Online Library for rules of use; OA articles are governed by the applicable Creative Commons License

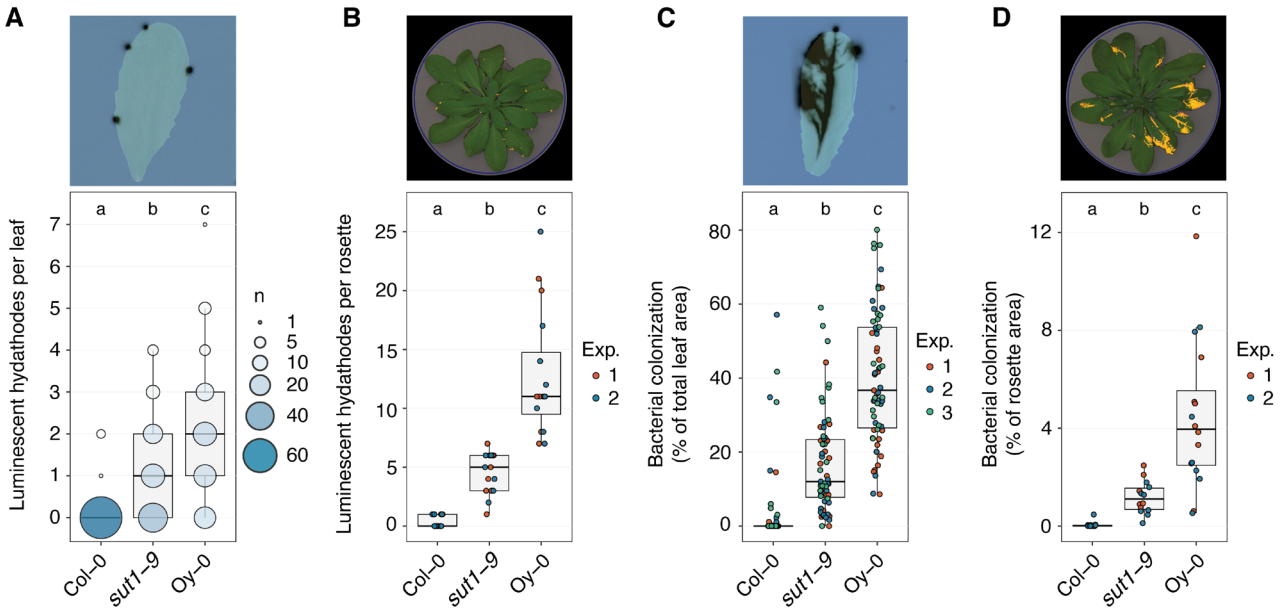

FIGURE 2 | Digital phenotyping of entire plants is consistent with results of detached leaf assays using *Xanthomonas campestris* pv. *campestris* (Xcc) Tn*7*:*lux* infection of three Arabidopsis lines with varying disease susceptibility. (A) Quantification of a *Xanthomonas* disease assay with detached leaves counting the number of hydathodes infected per leaf ($n = 63$ leaves per genotype). Leaves were imaged 7 days post-spray inoculation (dpi) with Xcc 8004 Δ*xopAC* Tn*7*:*Lux*. Letters above the box indicate different significance groups based on a nonparametric Kruskal–Wallis test followed by Dunn's post hoc test, $\alpha = 0.05$. (B) Same as panel (A), except that whole rosettes were digitally imaged ($n = 16$ plants per genotype) and represent an overlay of RGB and luminescence picture (luminescence shown in false colour). Each luminescent area is automatically highlighted by a red circle. Letters above the box indicate different significance groups based on a nonparametric Kruskal–Wallis test followed by Dunn's post hoc test, $\alpha = 0.05$. (C) Same as panel (A), except that proportion of the leaf area colonised by *Xanthomonas* is shown per detached leaf 14 dpi ($n = 63$ leaves per genotype). Significance letters from nonparametric Kruskal–Wallis test with Dunn's post hoc test, $\alpha = 0.05$. (D) Same as panel (A), except that relative rosette area colonised by *Xanthomonas* is shown using digital imaging of whole rosettes ($n = 16$ plants per genotype). Letters indicate significance groups based on a nonparametric Kruskal–Wallis test followed by Dunn's post hoc test, $\alpha = 0.05$. Coloured dots indicate data points from independent experiments.

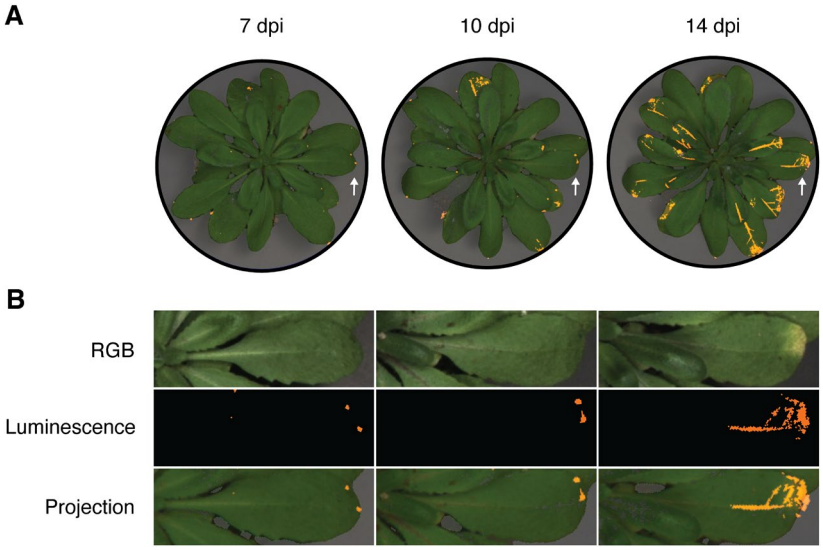

FIGURE 3 | Non-invasive phenotyping allows for tracking of *Xanthomonas* outbreaks from a single hydathode. (A) Imaging of *Xanthomonas campestris* pv. *campestris* (Xcc) Tn*7*:*lux* infections on Arabidopsis imaged at 7, 10 and 14 days post-inoculation (dpi) in the digital phenotyper. Luminescence is shown as false colour. White arrow marks a single leaf enlarged in (B). Individual luminescent areas are automatically marked with a red circle. (B) Enlarged images of leaf indicated in panel (A) showing Xcc outbreak from two individual hydathode infections in a single leaf.

heterologous effector delivery system (EDV) was used (Fabro et al. 2011). In this approach, Pst is used to secrete the Xcc type III effector (T3E) XopAC, as it triggers an immune response in Col-0 accession. This response restricts bacterial proliferation through recognition of XopAC by the RKS1-PBL2-ZAR1 resistosome (Guy et al. 2013; Wang et al. 2015, 2019). Similar to Xcc,

13643703, 2025, 2, Downloaded from https://bsppjournals.onlinelibrary.wiley.com/doi/10.1111/mpp.70055 by Uva Universiteitsbibliotheek, Wiley Online Library on [10/02/2025]. See the Terms and Conditions (https://onlinelibrary.wiley.com/terms-and-conditions) on Wiley Online Library for rules of use; OA articles are governed by the applicable Creative Commons License

Arabidopsis plants can be spray-inoculated using Pst DC3000 Tn*7:lux* and the luminescent signal can be imaged (Figure 4A). To quantify bacterial proliferation of Pst, we sprayed Col-0 wildtype plants and *rks1* and *zar1* knockout mutants (both in Col-0) with non-luminescent Pst, either wildtype or expressing *xopAC*, and determined the number of colony-forming units (CFU) in leaf discs of inoculated rosettes (Figure 4B). In wildtype Arabidopsis (Col-0), Pst expressing *xopAC* showed reduced bacterial proliferation at 3 dpi compared to the wildtype Pst. This reduced bacterial proliferation was not detected in the *zar1* and *rks1* knockout lines, indicating that host delivery of XopAC by the EDV system successfully triggered a ZAR1/RKS1-dependent immune response in wildtype Arabidopsis Col-0 plants. Next, to compare these results to the new image analysis pipeline, we sprayed the same Arabidopsis lines with Pst Tn*7:lux* (carrying either pEDV:*XopAC* or not) and quantified luminescence of whole rosettes (Figure 4C). The total bioluminescent area of Pst expressing x*opAC* was reduced in wildtype Col-0 plants but not in *zar1* and *rks1* knockout lines, suggesting that our digital phenotyping method consistently replicated the results of CFU counting. Therefore, we conclude that the phenotyping setup can also be applied to infer bacterial titres of mesophyll pathogens, highlighting the flexibility of the system.

3 | Discussion

Here, we present a non-invasive digital phenotyping method for quantification of plant disease symptoms and bacterial

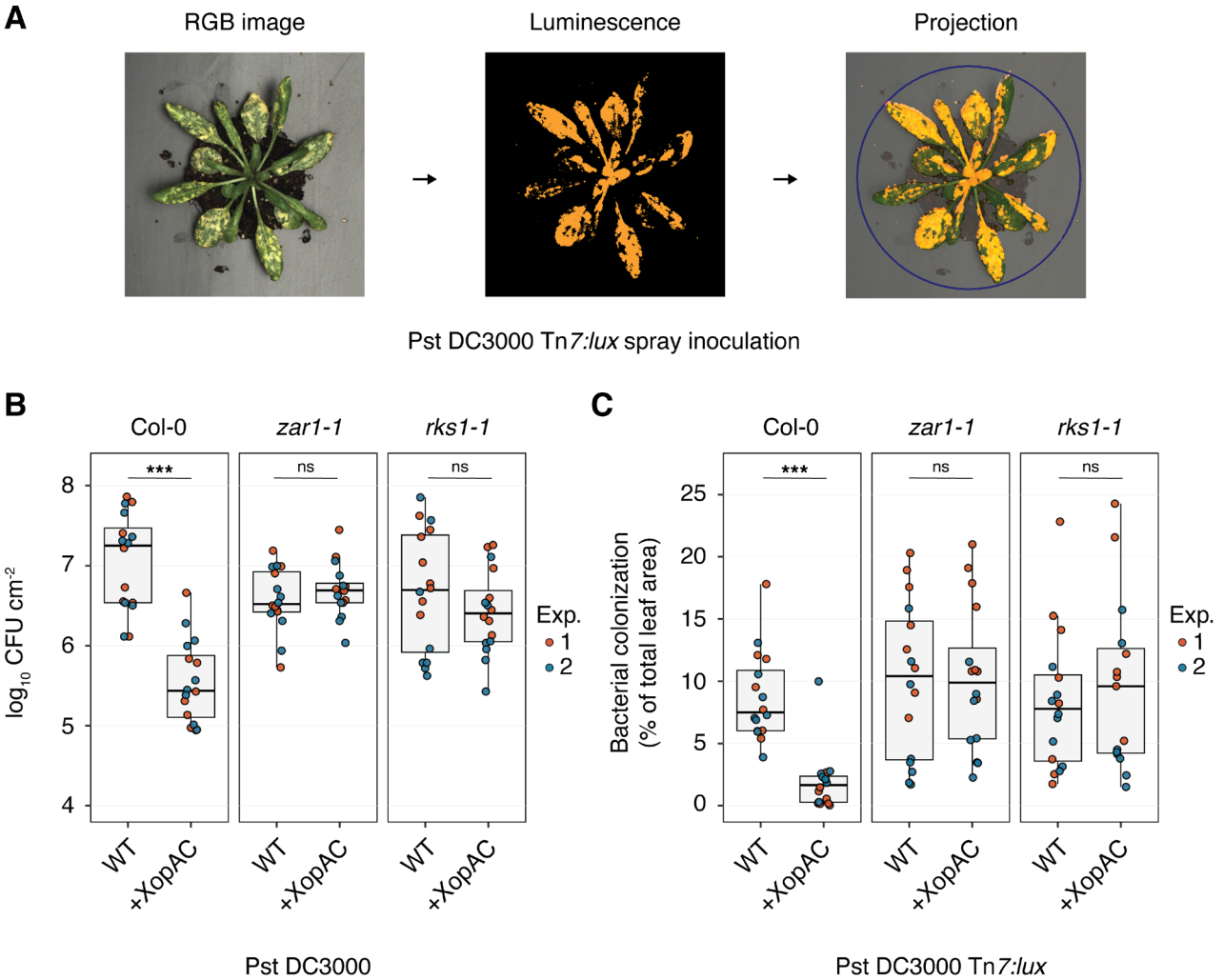

FIGURE 4 | Quantification of disease susceptibility for the mesophyll pathogen *Pseudomonas syringae* pv. *tomato* (Pst) using the digital phenotyping pipeline. (A) Example images taken with the digital phenotyper and output of the image analysis pipeline. Images were taken 5 days post-spray inoculation (5 dpi) with Pst DC3000 Tn*7:Lux* on Arabidopsis. (B) Disease severity measured as bacterial counts, that is, $\log_{10}$ CFU counts per cm^2 leaf at 3 days following spray inoculation with wildtype Pst DC3000 or carrying pEDV6:*XopAC* on wildtype Arabidopsis (Col-0) and the loss-of-function mutants *zar1* and *rks1* ($n = 16$ plants per treatment). XopAC-recognition in Col-0 leads to reduced bacterial titres when Pst expresses *xopAC*, while this immune recognition is compromised in *zar1* and *rks1*. Statistics on comparison between wildtype (WT) and + XopAC result from a Student's *t* test, $^{***}p \leq 0.001$, ns $p \geq 0.05$. (C) Bacterial colonisation of whole rosettes at 5 days following spray inoculation with Pst DC3000 Tn*7:Lux* (carrying pEDV6:*xopAC* or not) on Arabidopsis Col-0 WT, *zar1* and *rks1* knockout lines ($n = 16$ rosettes per treatment). Treatments and results are consistent with phenotyping method shown in (A). Significance on comparison between WT and + XopAC result from a nonparametric Wilcoxon rank test, $^{***}p \leq 0.001$, ns ≥ 0.05.

13643703, 2025, 2, Downloaded from https://bsppjournals.onlinelibrary.wiley.com/doi/10.1111/mpp.70055 by Uva Universiteitsbibliotheek, Wiley Online Library on [10/02/2025]. See the Terms and Conditions (https://onlinelibrary.wiley.com/terms-and-conditions) on Wiley Online Library for rules of use; OA articles are governed by the applicable Creative Commons License

spread using bioluminescent reporter strains. Previous efforts, including from our laboratory, have shed light on early hydathode infections using bioluminescent reporter strains (Cerutti et al. 2017; Paauw et al. 2023; Taks et al. 2024). We recently developed an automated image analysis pipeline, called ScAnalyzer, for analysing bacterial spread using detached leaves (Paauw et al. 2024). The approach presented here further improves this work by providing a method for non-invasive, highly automated phenotyping that yields accurate data on bacterial spread inside intact Arabidopsis rosettes (rather than only a single leaf). This digital phenotyping approach produces reproducible data that aligns with results obtained through conventional methods and is applicable to phytopathogenic bacteria that exhibit different infection strategies.

As shown in this work, our phenotyping setup can distinguish between several degrees of resistance against Xcc in Arabidopsis. This is important as many plant resistance mechanisms are quantitative in nature and polygenic (Corwin and Kliebenstein 2017). In addition, plant pathogens are known to evolve rapidly, resulting in the repeated emergence of resistance-breaking strains (de Wit 2016; Di et al. 2017; Lenman et al. 2016). Therefore, being able to better screen for partial or quantitative resistance could provide novel genetic sources to stack different resistance genes against plant pathogens. In addition to acquiring highly accurate phenotyping data for both the plant and the pathogen, the setup is also suited to screen large Arabidopsis populations. As 16 plants can be imaged within 5 min, this allows for non-invasive screening of hundreds of plants in a single day, offering a significant reduction in labour over our previously reported method using light-sensitive films, while increasing our image resolution and avoiding a potential bias in leaf sampling (Paauw et al. 2024). The image analysis pipeline is adjustable to other tray formats, allowing the simultaneous screening of up to 40 plants when younger Arabidopsis plants are imaged, increasing the throughput even further. In this way, we can tap into the large reservoir of natural variation for Arabidopsis to screen for additional sources of resistance (Weigel and Mott 2009). Many previously reported methods for the detection of bioluminescent pathogens in plants are limited to assessing several leaves or plants at a time (Mutka et al. 2016; Wang et al. 2024; Xu et al. 2022). Furthermore, besides placing plants in the imaging device, the imaging setup and subsequent analysis pipeline both require little to no additional work, paving the way for implementation in a conveyer belt-like plant pathogen phenotyping platform.

In a complex multistage interaction between a plant host and its pathogen, such as Xcc infecting Arabidopsis, gaining knowledge on the different stages (i.e., hydathode, vasculature, mesophyll) provides a more holistic view on the entire disease cycle. For example, plant immune responses against Xcc occur as early as the hydathode colonisation (Cerutti et al. 2017; Paauw et al. 2023; Taks et al. 2024), but also in the vasculature (Lin et al. 2022; Xie et al. 2023) and mesophyll tissue (Wang et al. 2015). The here-described phenotyping platform is able to record plant resistance at individual stages of the Xcc infection or to perform, for example, genome-wide association studies (GWAS) screening for candidate susceptibility genes. Moreover, the option of tracking a single infection event over time provides the possibility to investigate the mechanism underpinning bacterial escape from the hydathode towards the xylem.

While this setup was designed to study the spatial and temporal colonisation of the highly specialised vascular plant pathogen Xcc, we also show its versatility by unveiling the resistance response against the model plant pathogen Pst infecting the leaf mesophyll (Xin, Kvitko, and He 2018). Using the same parameters as for the quantification of Xcc in later stages of infection (i.e., the mesophyll stage), we accurately recapitulate the earlier reported differences in resistance levels between several well-characterised Arabidopsis mutant lines through both CFU counts following syringe inoculation and bioluminescence after spray inoculation (Figure 4). This is in agreement with earlier work, in which a direct and linear correlation was found between Pst bacterial densities and the bioluminescent signal in planta (Fan, Crooks, and Lamb 2008; Pujara et al. 2021). Another study confirmed that Tn*7*:*lux* insertions in *P. syringae* pv. *phaseolicola* did not affect bacterial growth and virulence during infections of common bean (Soldan et al. 2021). However, bioluminescence-based approaches typically suffer from reduced sensitivity compared to CFU-based methods (van Hulten, Chatterjee, and van den Burg 2019), meaning that subtle differences in bacterial densities could be overlooked. While it is important to consider that luminescence depends on the metabolic activity of bacteria (Paauw et al. 2023; van Hulten, Chatterjee, and van den Burg 2019), we did not detect a large impact of growth phase on luminescent signal in an in vitro growth experiment (Figure S3). In addition, we use bacterial spread as an indicator for disease progression in our approach, rather than directly inferring bacterial densities in planta from bioluminescence. Therefore, while bioluminescent approaches may lack the sensitivity needed to accurately determine total bacterial densities over a wide detection range, they do provide valuable insights into the spatiotemporal dynamics of bacterial colonisation. This makes it a very useful method to study the bacterial colonisation in the context of a systemic infection over time. In addition, the possibility of high-throughput screening is a clear advantage over CFU-based methods. Thus, this system provides ample opportunity to study other pathogens that can be genetically tagged with bioluminescence, such as other *Pseudomonas* species and *Ralstonia solanacearum* (Jutras et al. 2021; Mutka et al. 2016; Xu et al. 2022). Altogether, with this setup, it is feasible to gain more detailed knowledge on the complex infection strategies used by bacterial pathogens of Arabidopsis.

Although the Python-based image analysis pipeline has been optimised for this specific imaging cabinet and the interaction between Xcc and Arabidopsis, several aspects of the pipeline make it compatible with other systems and other plant–pathogen systems. While the base requirement remains the input of an RGB image and binary output of a CCD camera, the user-adjustable settings allow for different light conditions and plant layout, while the camera calibration matrix allows for application in different imaging cabinets. Thus, the analysis pipeline could be implemented with minor adjustments based on the specific imaging devices used and the model system.

13643703, 2025, 2, Downloaded from https://bsppjournals.onlinelibrary.wiley.com/doi/10.1111/mpp.70055 by Uva Universiteitsbibliotheek, Wiley Online Library on [10/02/2025]. See the Terms and Conditions (https://onlinelibrary.wiley.com/terms-and-conditions) on Wiley Online Library for rules of use; OA articles are governed by the applicable Creative Commons License

4 | Experimental Procedures

4.1 | Imaging Cabinet Specifications

The PhenoAIxpert imaging cabinet (600 × 600 × 1115 mm L × W × H) was ordered from LemnaTec GmbH (Aachen, Germany). The default version comes with a fitted 12-megapixel RGB industrial camera (Allied Vision Manta G12136, 4112 × 3008 pixels) for imaging of plants. This cabinet was custom fitted with a 4-megapixel Raptor Eagle V 4240 CCD camera (2084 × 2084 pixels, pixel size 13.5 × 13.5 μm) with a Zeiss Milvus 1.4 × 35 mm lens. The two cameras were placed adjacent at the same height from the imaging platform. Focus depth of both cameras was adjusted manually for both cameras to ensure optimal focus depth at the imaging plane of Arabidopsis rosettes.

4.2 | Plant Growth Conditions

All Arabidopsis lines used are listed in Table S2. For all experiments, seeds were stratified for 3–4 days on wet filter paper at 4°C in the dark and then sown in 40-pot trays (Desh Plantpak, Tray Danish size 40-cell [8 × 5]) in slitpots (Pöppelmann Teku, S 5,5 LB), using potting soil (Jongkind Substrates, Hol80 zaaigrond Nr 1) to which 500 mL Entonem suspension (Koppert Biological Systems, c. 1.6×10^6 third-stage *Steinernema feltiae* nematode larvae) was added per tray. Hereafter, trays were placed in short-day conditions (11/13 h light/dark, 22°C, RH 70%). For the first 4–5 days, the trays were covered with a transparent plastic dome to ensure uniform germination.

4.3 | Plasmid and Transgenic Strain Generation

All bacterial strains, plasmids and oligonucleotides used are listed in Table S2. Bacterial strains were tagged with a double bioluminescence/fluorescence cassette using the mini-Tn*7* transposon system (Choi and Schweizer 2006; Soldan et al. 2021). Recipient strains (Xcc8004 Δ*xopAC* or Pst DC3000) were co-incubated on Luria Bertani (LB) plates with one donor *Escherichia coli* strain (DH5α + pRS-Tn*7*-pNPTII::*lux-pA1::mTq2*; Paauw et al. 2023; Soldan et al. 2021) and two helper *E. coli* strains; one carrying Tn*7* transposon genes *tns-ABCDE* (DH5α + pUX-BF13; Bao et al. 1991) and one carrying a plasmid that facilitates conjugation (HB101 + pRK2073; Figurski and Helinski 1979). Next, cultures were collected and transformants were selected on LB plates with antibiotics (10 μg/mL gentamicin and 50 μg/mL nitrofurantoin) and checked for luminescence using the ChemiDoc MP imager (Bio-Rad).

To create the pEDV6 (Fabro et al. 2011) vector carrying Xcc 8004 *xopAC*, Xcc genomic DNA was isolated using the QIAGEN Puregene DNA-isolation kit for gram-negative bacteria. Hereafter, the *xopAC* coding sequence was amplified using primers that contain *attB* sites for Gateway cloning. The amplified product was then cloned into pEDV6 by LR reaction creating pEDV6:*xopAC*. The resulting vector was transformed into Pst DC3000 by electroporation (Choi, Kumar, and Schweizer 2006).

4.4 | Plate Reader Assay

To determine the effect of the Tn*7* insertion and expression of the luminescence cassette on bacterial growth, in vitro growth curves of all Tn*7*:*lux* strains were monitored in a plate reader (Agilent BioTek Synergy H1MF) for 24 h. Cultures of Xcc (wild type [WT] and Tn*7*:*lux*) and Pst (WT and Tn*7*:*lux*) were grown overnight at 28°C with shaking at 200 rpm in 10 mL liquid Kado and King's B (KB), respectively. Next, cultures were centrifuged (3500 *g* for 5 min), washed once with sterile medium and then diluted to $OD_{600} = 0.2$ and grown for an additional 3 h until the cultures reached the exponential phase ($OD_{600} = 0.4–0.6$). Then, cultures were diluted to $OD_{600} = 0.005$ and 150 μL (six replicates per strain) was added per well in a black 96-well plate with transparent bottom. Luminescence and OD_{600} were monitored every 15 min over a 24-h period with continuous shaking at 28°C.

4.5 | *Xanthomonas* Disease Assays

Spray inoculations with bioluminescent Xcc8004 Δ*xopAC* Tn*7*:*lux-mTq2* (Xcc Tn*7*:*lux*) were performed as previously described (Paauw et al. 2023; van Hulten, Chatterjee, and van den Burg 2019). Xcc strains were plated on Kado agar (Kado and Heskett 1970) with antibiotics (10 μg/mL gentamicin and 50 μg/mL nitrofurantoin) and allowed to grow for 48–72 h at 28°C. Bacteria were collected, washed once with 10 mM $MgSO_4$ and diluted to $OD_{600} = 0.1$. Silwet L-77 was added to a final concentration of 0.0002% and bacteria were sprayed on 4- to 5-week-old Arabidopsis plants (Preval sprayer, SKU# 0221). To promote natural infection, sprayed plants were subjected to two guttation cycles over 2 days in a climate chamber (Snijders Labs, MC1000) (van Hulten, Chatterjee, and van den Burg 2019) and subsequently grown for an additional 12 days at short daylight cycle (11/13 h light/dark) at 24°C–22°C with RH 70% in the same chamber.

To quantify hydathode infections and bacterial colonisation using light-sensitive film, at 7 and 14 dpi, the three most symptomatic leaves of each plant were taken and glued onto paper (A3 paper size) with a printed grid and covered with a transparent plastic sheet. Next, a light-sensitive X-ray film (Fuji Super RX) was placed on top and left for exposure overnight (van Hulten, Chatterjee, and van den Burg 2019). The film was developed the next morning and scanned, alongside the leaves, in an A3 flatbed scanner (Epson Expression 12000XL). For 7 dpi samples, images were overlayed in Adobe Photoshop 2023/2024 to count luminescent hydathodes per leaf. At 14 dpi, scans of leaves and light-sensitive film were analysed using the ScAnalyzer image analysis tool (Paauw et al. 2024) to quantify both the level of chlorosis and bacterial spread.

4.6 | *Pseudomonas* Disease Assays

For both spray inoculations and infiltrations, Pst was grown overnight in 50 mL Falcon tubes containing 20 mL KB medium at 28°C and 200 rpm. The next day, cultures were centrifuged, washed once with 10 mM $MgSO_4$ and diluted to $OD_{600} = 0.1$ for spray inoculations or $OD_{600} = 0.001$ for infiltrations. For spray assays, Silwet L-77 was added to a final concentration of 0.002%.

13643703, 2025, 2, Downloaded from https://bsppjournals.onlinelibrary.wiley.com/doi/10.1111/mpp.70055 by Uva Universiteitsbibliotheek, Wiley Online Library on [10/02/2025]. See the Terms and Conditions (https://onlinelibrary.wiley.com/terms-and-conditions) on Wiley Online Library for rules of use; OA articles are governed by the applicable Creative Commons License

Next, 4- to 5-week-old Arabidopsis plants were sprayed (Preval sprayer, SKU# 0221) or pressure-infiltrated using a blunt syringe. Infected plants were grown for 5 days at short-day conditions (11/13 h light/dark, 24°C–22°C, RH 70%). The first 3 days, plants were covered with a transparent plastic dome to promote infection.

To determine CFU counts after leaf infiltration, at 3 dpi, two leaf discs (5 mm diameter) were taken from each infiltrated leaf with a leaf puncher, placed into 500 µL 10 mM $MgSO_4$ containing two steel beads and homogenised twice for 1 min at 30 Hz in a TissueLyser II (QIAGEN). Samples were serially diluted and plated in duplicates on KB agar plates containing 10 µg/mL gentamicin and 25 µg/mL rifampicin antibiotics. After 24 h, colonies were counted and log CFU per cm^2 leaf material (log_{10} CFU cm^{-2}) was calculated.

4.7 | Disease Quantification With Digital Phenotyper

At 7 and 14 dpi (Xcc) or 3 and 5 dpi (Pst), plants in slit pots were taken from their respective locations in the 40-pot tray and placed into an anodized (black) aluminium tray with 16 (4×4) positions for imaging (Figure S1B). Next, the plants were covered with a black plastic lid and kept in the dark for 5 min to reduce photosynthetic background signal when imaging luminescence. Hereafter, the imaging tray was placed in the digital phenotyper and was imaged in a standard program (300 s exposure CCD camera and 70 ms exposure RGB camera). Raw images (RGB and CCD) were exported and fed into our image analysis pipeline.

4.8 | Automated Image Analysis

Raw images are processed by an in-house developed Python analysis pipeline that uses the open-source OpenCV Library for image analysis (Bradski and Kaehler 2000). In this pipeline, rosettes are detected in the RGB image according to user-adjustable HSV values for leaf tissue. The user can define row and column numbers, indicating the number of rosettes to be found in the image. A sorting algorithm then orders the rosettes and assigns row and column numbers. Whenever fewer rosettes are detected than initially defined, the RGB image is brightened and saturated to increase detection capabilities of the algorithm. Next, each rosette contour is drawn and masked to select only plant tissues and no background (e.g., soil or tray). For each masked rosette, several output parameters are calculated, including rosette area, green area and yellow area based on user-defined colour parameters. A smallest-enclosing circle is then drawn around each rosette mask to create a mask for the luminescence image. The luminescence image is overlayed onto the RGB image using the homography matrix, aligning both RGB and CCD cameras, and for each smallest-enclosing circle, the number of luminescent objects (corresponding to colonised hydathodes [Xcc: 7 DPI]) and/or total luminescence signal (Pst: 3 and 5 DPI, Xcc: 14 DPI) is calculated. Metadata on each rosette (plant genotype, treatment, etc.) can then be matched to all measurement values and combined into a data output file. All code and instructions on parameter selection and how to perform the image analysis are freely available on GitHub (https://github.com/MolPlantPathology/Digital_phenotyper).

4.9 | Quantification and Statistical Analyses

All data analyses and plotting were done in R (v. 4.3.2). For statistical analysis of parametric data, a two-way analysis of variance followed by a Tukey post hoc test was performed for multiple comparisons between groups and a Student's *t* test when comparing two groups. For nonparametric data, such as hydathode counts or proportional data, a Kruskal–Wallis test followed by a Dunn's post hoc test was performed for multiple comparisons and a Wilcoxon test when comparing two groups. All experiments were performed in at least two independent repetitions with similar results. Data from repetitions was pooled for visualisation and statistical analysis.

Acknowledgements

The authors would like to thank Ludek Tikovsky and Harold Lemereis for excellent plant care in the greenhouse. Also, we would like to thank Dominique Roby and Darrell Desveaux for sharing Arabidopsis mutant lines and Alan Collmer, Gail Preston and Laurent Noël for sharing bacterial strains and plasmids. Lastly, we would like to thank LemnaTec for the assistance in designing the digital phenotyper. This research was supported by the Topsector T&U TKI programs 'Stop natural entry' and 'Finding the Achilles' heel of Brassica for Black Rot disease' (grants EZ-2012-02 and TU18024 to H.A.v.d.B.), an NWO-XS grant (OCENW.XS24.1.155 to S.P.) and the breeding companies Bejo Zaden B.V. and Rijk Zwaan.

Conflicts of Interest

The authors declare no conflicts of interest.

Data Availability Statement

The data that support the findings of this study is available from the corresponding author upon reasonable request.

References

Bao, Y., D. P. Lies, H. Fu, and G. P. Roberts. 1991. "An Improved Tn7-Based System for the Single-Copy Insertion of Cloned Genes Into Chromosomes of Gram-Negative Bacteria." *Gene* 109: 167–168. https://doi.org/10.1016/0378-1119(91)90604-A.

Bradski, G., and A. Kaehler. 2000. "OpenCV. Dr Dobb's J. Softw. Tools 3."

Cerutti, A., A. Jauneau, M.-C. Auriac, et al. 2017. "Immunity at Cauliflower Hydathodes Controls Systemic Infection by *Xanthomonas campestris* pv. *campestris*." *Plant Physiology* 174: 700–716. https://doi.org/10.1104/pp.16.01852.

Choi, K.-H., A. Kumar, and H. P. Schweizer. 2006. "A 10-Min Method for Preparation of Highly Electrocompetent *Pseudomonas aeruginosa* Cells: Application for DNA Fragment Transfer Between Chromosomes and Plasmid Transformation." *Journal of Microbiological Methods* 64: 391–397. https://doi.org/10.1016/j.mimet.2005.06.001.

Choi, K.-H., and H. P. Schweizer. 2006. "Mini-Tn7 Insertion in Bacteria With Single attTn7 Sites: Example *Pseudomonas aeruginosa*." *Nature Protocols* 1: 153–161. https://doi.org/10.1038/nprot.2006.24.

Corwin, J. A., and D. J. Kliebenstein. 2017. "Quantitative Resistance: More Than Just Perception of a Pathogen." *Plant Cell* 29: 655–665. https://doi.org/10.1105/tpc.16.00915.

13643703, 2025, 2, Downloaded from https://bsppjournals.onlinelibrary.wiley.com/doi/10.1111/mpp.70055 by Uva Universiteitsbibliotheek, Wiley Online Library on [10/02/2025]. See the Terms and Conditions (https://onlinelibrary.wiley.com/terms-and-conditions) on Wiley Online Library for rules of use; OA articles are governed by the applicable Creative Commons License

de Wit, P. J. G. M. 2016. "*Cladosporium fulvum* Effectors: Weapons in the Arms Race With Tomato." *Annual Review of Phytopathology* 54: 1–23. https://doi.org/10.1146/annurev-phyto-011516-040249.

Di, X., L. Cao, R. K. Hughes, N. Tintor, M. J. Banfield, and F. L. W. Takken. 2017. "Structure-Function Analysis of the *Fusarium oxysporum* Avr2 Effector Allows Uncoupling of Its Immune-Suppressing Activity From Recognition." *New Phytologist* 216: 897–914. https://doi.org/10.1111/nph.14733.

Fabro, G., J. Steinbrenner, M. Coates, et al. 2011. "Multiple Candidate Effectors From the Oomycete Pathogen *Hyaloperonospora arabidopsidis* Suppress Host Plant Immunity." *PLoS Pathogens* 7: e1002348. https://doi.org/10.1371/journal.ppat.1002348.

Fan, J., C. Crooks, and C. Lamb. 2008. "High-Throughput Quantitative Luminescence Assay of the Growth in Planta of *Pseudomonas syringae* Chromosomally Tagged With *Photorhabdus luminescens luxCDABE*." *Plant Journal* 53: 393–399. https://doi.org/10.1111/j.1365-313X.2007.03303.x.

Feng, F., F. Yang, W. Rong, et al. 2012. "A *Xanthomonas* Uridine 5′-Monophosphate Transferase Inhibits Plant Immune Kinases." *Nature* 485: 114–118. https://doi.org/10.1038/nature10962.

Figurski, D. H., and D. R. Helinski. 1979. "Replication of an Origin-Containing Derivative of Plasmid RK2 Dependent on a Plasmid Function Provided in Trans." *Proceedings of the National Academy of Sciences of the United States of America* 76: 1648–1652. https://doi.org/10.1073/pnas.76.4.1648.

Furci, L., D. Pascual-Pardo, and J. Ton. 2021. "A Rapid and Non-destructive Method for Spatial–Temporal Quantification of Colonization by *Pseudomonas syringae* pv. *tomato* DC3000 in *Arabidopsis* and Tomato." *Plant Methods* 17: 126. https://doi.org/10.1186/s13007-021-00826-2.

Guy, E., M. Lautier, M. Chabannes, et al. 2013. "xopAC-Triggered Immunity Against *Xanthomonas* Depends on *Arabidopsis* Receptor-Like Cytoplasmic Kinase Genes *PBL2* and *RIPK*." *PLoS One* 8: e73469. https://doi.org/10.1371/journal.pone.0073469.

Hugouvieux, V., C. E. Barber, and M. J. Daniels. 1998. "Entry of *Xanthomonas campestris* pv. *campestris* Into Hydathodes of *Arabidopsis thaliana* Leaves: A System for Studying Early Infection Events in Bacterial Pathogenesis." *Molecular Plant–Microbe Interactions* 11: 537–543. https://doi.org/10.1094/MPMI.1998.11.6.537.

Jian, Y., D. Gong, Z. Wang, et al. 2024. "How Plants Manage Pathogen Infection." *EMBO Reports* 25: 31–44. https://doi.org/10.1038/s44319-023-00023-3.

Jutras, P. V., R. Soldan, I. Dodds, M. Schuster, G. M. Preston, and R. A. L. van der Hoorn. 2021. "AgroLux: Bioluminescent *Agrobacterium* to Improve Molecular Pharming and Study Plant Immunity." *Plant Journal* 108: 600–612. https://doi.org/10.1111/tpj.15454.

Kado, C. I., and M. G. Heskett. 1970. "Selective Media for Isolation of *Agrobacterium*, *Corynebacterium*, *Erwinia*, *Pseudomonas* and *Xanthomonas*." *Phytopathology* 60: 969–976. https://doi.org/10.1094/Phyto-60-969.

Laflamme, B., M. Middleton, T. Lo, D. Desveaux, and D. S. Guttman. 2016. "Image-Based Quantification of Plant Immunity and Disease." *Molecular Plant–Microbe Interactions* 29: 919–924. https://doi.org/10.1094/MPMI-07-16-0129-TA.

Lenman, M., A. Ali, P. Mühlenbock, et al. 2016. "Effector-Driven Marker Development and Cloning of Resistance Genes Against *Phytophthora infestans* in Potato Breeding Clone SW93-1015." *Theoretical and Applied Genetics* 129: 105–115. https://doi.org/10.1007/s00122-015-2613-y.

Lin, H., M. Wang, Y. Chen, et al. 2022. "An MKP-MAPK Protein Phosphorylation Cascade Controls Vascular Immunity in Plants." *Science Advances* 8: eabg8723. https://doi.org/10.1126/sciadv.abg8723.

Melotto, M., L. Zhang, P. R. Oblessuc, and S. Y. He. 2017. "Stomatal Defense a Decade Later." *Plant Physiology* 174: 561–571. https://doi.org/10.1104/pp.16.01853.

Meyer, D., E. Lauber, D. Roby, M. Arlat, and T. Kroj. 2005. "Optimization of Pathogenicity Assays to Study the *Arabidopsis thaliana–Xanthomonas campestris* pv. *campestris* Pathosystem." *Molecular Plant Pathology* 6: 327–333. https://doi.org/10.1111/j.1364-3703.2005.00287.x.

Mutka, A. M., S. J. Fentress, J. W. Sher, et al. 2016. "Quantitative, Image-Based Phenotyping Methods Provide Insight Into Spatial and Temporal Dimensions of Plant Disease." *Plant Physiology* 172: 650–660. https://doi.org/10.1104/pp.16.00984.

Paauw, M., G. Hardeman, N. W. Taks, et al. 2024. "ScAnalyzer: An Image Processing Tool to Monitor Plant Disease Symptoms and Pathogen Spread in *Arabidopsis thaliana* Leaves." *Plant Methods* 20: 80. https://doi.org/10.1186/s13007-024-01213-3.

Paauw, M., M. van Hulten, S. Chatterjee, et al. 2023. "Hydathode Immunity Protects the *Arabidopsis* Leaf Vasculature Against Colonization by Bacterial Pathogens." *Current Biology* 33: 697–710.e6. https://doi.org/10.1016/j.cub.2023.01.013.

Pujara, D. S., S.-I. Kim, J. C. Nam, et al. 2021. "Imaging-Based Resistance Assay Using Enhanced Luminescence-Tagged *Pseudomonas syringae* Reveals a Complex Epigenetic Network in Plant Defense Signaling Pathways." *Molecular Plant–Microbe Interactions* 34: 990–1000. https://doi.org/10.1094/MPMI-12-20-0351-TA.

Simon, M., O. Loudet, S. Durand, et al. 2008. "Quantitative Trait Loci Mapping in Five New Large Recombinant Inbred Line Populations of *Arabidopsis thaliana* Genotyped With Consensus Single-Nucleotide Polymorphism Markers." *Genetics* 178: 2253–2264. https://doi.org/10.1534/genetics.107.083899.

Soldan, R., N. Sanguankiattichai, M. Bach-Pages, I. Bervoets, W. E. Huang, and G. M. Preston. 2021. "From Macro to Micro: A Combined Bioluminescence-Fluorescence Approach to Monitor Bacterial Localization." *Environmental Microbiology* 23: 2070–2085. https://doi.org/10.1111/1462-2920.15296.

Taks, N. W., M. Van Hulten, J. A. Van Splunter-Berg, et al. 2024. "Hydathode Immunity Against the Vascular Pathogen *Xanthomonas campestris* pv. *campestris* by the *Arabidopsis* CNL-Type Receptor SUT1." *bioRxiv* 2024.06.20.599835. https://doi.org/10.1101/2024.06.20.599835. [Preprint].

Tornero, P., and J. L. Dangl. 2001. "A High-Throughput Method for Quantifying Growth of Phytopathogenic Bacteria in *Arabidopsis thaliana*." *Plant Journal* 28: 475–481. https://doi.org/10.1046/j.1365-313X.2001.01136.x.

Van de Weyer, A.-L., F. Monteiro, O. J. Furzer, et al. 2019. "A Species-Wide Inventory of NLR Genes and Alleles in *Arabidopsis thaliana*." *Cell* 178: 1260–1272. e14. https://doi.org/10.1016/j.cell.2019.07.038.

van Hulten, M., S. Chatterjee, and H. A. van den Burg. 2019. "Infection Assay for *Xanthomonas campestris* pv. campestris in *Arabidopsis thaliana* Mimicking Natural Entry via Hydathodes." in: *Plant Innate Immunity*, 159–185. New York, NY: Springer, Humana. https://doi.org/10.1007/978-1-4939-9458-8_16.

Velásquez, A. C., M. Oney, B. Huot, S. Xu, and S. Y. He. 2017. "Diverse Mechanisms of Resistance to *Pseudomonas syringae* in a Thousand Natural Accessions of *Arabidopsis thaliana*." *New Phytologist* 214: 1673–1687. https://doi.org/10.1111/nph.14517.

Wang, G., B. Roux, F. Feng, et al. 2015. "The Decoy Substrate of a Pathogen Effector and a Pseudokinase Specify Pathogen-Induced Modified-Self Recognition and Immunity in Plants." *Cell Host & Microbe* 18: 285–295. https://doi.org/10.1016/j.chom.2015.08.0.

Wang, H., S. Song, S. Gao, et al. 2024. "The NLR Immune Receptor ADR1 and Lipase-Like Proteins EDS1 and PAD4 Mediate Stomatal Immunity in *Nicotiana benthamiana* and *Arabidopsis*." *Plant Cell* 36: 427–446. https://doi.org/10.1093/plcell/koad270.

Wang, J., M. Hu, J. Wang, et al. 2019. "Reconstitution and Structure of a Plant NLR Resistosome Conferring Immunity." *Science* 364: eaav5870. https://doi.org/10.1126/science.aav5870.

13643703, 2025, 2, Downloaded from https://bsppjournals.onlinelibrary.wiley.com/doi/10.1111/mpp.70055 by Uva Universiteitsbibliotheek, Wiley Online Library on [10/02/2025]. See the Terms and Conditions (https://onlinelibrary.wiley.com/terms-and-conditions) on Wiley Online Library for rules of use; OA articles are governed by the applicable Creative Commons License

Weigel, D., and R. Mott. 2009. "The 1001 Genomes Project for *Arabidopsis thaliana*." *Genome Biology* 10: 1–5. https://doi.org/10.1186/gb-2009-10-5-107.

Whalen, M. C., R. W. Innes, A. F. Bent, and B. J. Staskawicz. 1991. "Identification of *Pseudomonas syringae* Pathogens of *Arabidopsis* and a Bacterial Locus Determining Avirulence on Both *Arabidopsis* and Soybean." *Plant Cell* 3: 49–59. https://doi.org/10.1105/tpc.3.1.49.

Winson, M. K., S. Swift, P. J. Hill, et al. 1998. "Engineering the *luxCDABE* Genes From *Photorhabdus luminescens* to Provide a Bioluminescent Reporter for Constitutive and Promoter Probe Plasmids and Mini-Tn*5* Constructs." *FEMS Microbiology Letters* 163: 193–202. https://doi.org/10.1111/j.1574-6968.1998.tb13045.x.

Xie, Q., B. Wei, Z. Zhan, et al. 2023. "*Arabidopsis* Membrane Protein AMAR1 Interaction With Type III Effector XopAM Triggers a Hypersensitive Response." *Plant Physiology* 193: 2768–2787. https://doi.org/10.1093/plphys/kiad478.

Xin, X.-F., B. Kvitko, and S. Y. He. 2018. "*Pseudomonas syringae*: What It Takes to Be a Pathogen." *Nature Reviews Microbiology* 16: 316–328. https://doi.org/10.1038/nrmicro.2018.17.

Xu, C., L. Zhong, Z. Huang, et al. 2022. "Real-Time Monitoring of *Ralstonia solanacearum* Infection Progress in Tomato and *Arabidopsis* Using Bioluminescence Imaging Technology." *Plant Methods* 18: 7. https://doi.org/10.1186/s13007-022-00841-x.

Supporting Information

Additional supporting information can be found online in the Supporting Information section.

13643703, 2025, 2, Downloaded from https://bsppjournals.onlinelibrary.wiley.com/doi/10.1111/mpp.70055 by Uva Universiteitsbibliotheek, Wiley Online Library on [10/02/2025]. See the Terms and Conditions (https://onlinelibrary.wiley.com/terms-and-conditions) on Wiley Online Library for rules of use; OA articles are governed by the applicable Creative Commons License